Thin $YBa_2Cu_3O_{7-\delta}$ patterns by Chemical Solution Processing using Ink-Jet Printing

Jonas Feys[1], Bram Ghekiere[1], Petra Lommens[1], Simon C. Hopkins[2], Pieter Vermeir[1,3], Michael Baecker[4], Bartek A. Glowacki[2,5,6], Isabel Van Driessche[1]

[1] SCRiPTS, Ghent University, Ghent, Belgium
[2] ASCG, Department of Materials Science and Metallurgy, University of Cambridge, Cambridge CB2 3QZ, UK
[3] Department of Industrial Sciences; University College Ghent; Ghent; Belgium
[4] Deutsche Nanoschicht GmbH, Rheinbach, Germany
[5] Department of Physics and Energy, University of Limerick, Ireland
[6] Institute of Power Engineering, ul Augustowka 6, 02-981 Warsaw, Poland

ABSTRACT

In this paper, we present ink-jet printing as an attractive alternative to lithography and etching methods for the development of multi-filamentary $YBa_2Cu_3O_{7-\delta}$ coated conductors. Our research is mainly focused on the study of the influence of rheological parameters on the printability of water-based inks in order to produce superconducting patterns on $SrTiO_3$ and CeO_2-$La_2Zr_2O_7$-Ni5at%W substrates. An aqueous YBCO precursor ink with a total metal ion concentration of 1.1 mol/L with a viscosity of 6.79 mPa s and a surface tension of 67.9 mN/m is developed. Its printing behavior using several ink-jet printing devices is verified using a camera with strobed illumination to quantify droplet velocity and volume. After optimization of the deposition parameters, YBCO tracks with different dimensions could be printed on both types of substrates. Their shape and dimensions were determined using optical microscopy and non-contact profilometry, showing 100-200 nm thick and 40-200 µm wide tracks. Finally, resistivity measurements were performed on the widest tracks on $SrTiO_3$ showing a clear drop in the resistivity starting from 88.6 K with a ΔT_c of 1.4 K.

INTRODUCTION

In recent years, several companies have developed technologies for the processing of long lengths of $YBa_2Cu_3O_{7-\delta}$ (YBCO) coated conductors [1-5]. One common coated conductor design consists of a well textured Ni-5at%W substrate, covered by a buffer layer architecture topped with a continuous superconducting film. These conductors can be wound as coils and, when used in motors and generators instead of copper wires, they can reduce the total size and weight of the device because of their ability to carry high currents without resistance. Yet, these coated conductors produce large losses when used with alternating current (AC) or fields [6-9]. The high aspect ratio of the coated conductor geometry leads to high hysteresis losses proportional to the width of the superconducting film. These losses can be effectively reduced by dividing the superconducting film into narrow filaments, with the net hysteresis losses ideally inversely proportional to the number of filaments. In practice, the total AC losses of a striated superconducting tape contain other contributions which would also need to be considered in a coated conductor optimized for AC applications. There will always be eddy current losses associated with substrate and stabilization layers, which can be reduced by maximizing the substrate resistance and by also striating the stabilization layer. These methods, and avoiding

interfilamentary bridging, also reduce coupling currents; but twisting the conductor, or ideally fully transposing the filaments, is required to minimize coupling losses [10-18].
This filamentary superconducting structure can be accomplished through several techniques which can be divided into two main approaches: with or without material removal. Lithography, wet chemical etching, ion beam etching, laser ablation or slitting of the tape are techniques where superconducting material is removed [7, 8, 12, 19-21]. They have a variety of disadvantages such as high cost, local degradation of the superconducting properties or tape fragmentation. The other class of techniques allows direct patterning of the superconductor through electrodeposition or drop-on-demand (DOD) inkjet printing [22-26]. While ink-jet printing has been used for many years in depositing text or patterns on textiles or paper, it is only recently that there has been a growing interest in using the deposition technique for functional ceramic coatings and structures [27-31]. The biggest advantage of ink-jet printing as a one-step process is its low investment cost, scalability, the more efficient use of materials and the good control of the thickness and pattern of the coating.
In this paper, we show that by combining the ink-jet printing method with completely water-based inks, containing non-hazardous metal salts as precursor materials, it is possible to print multi-filamentary superconducting YBCO patterns. Avoiding the incorporation of F-containing components results in a faster and environmentally more benign production method. By controlling the wetting behavior of the ink on appropriate substrates, it becomes possible to predict pattern dimensions. Therefore, both the droplet diameter after ejection from the printing nozzle and contact angle after contacting the substrate need to be known. The droplet diameter is mainly dependent on the opening of the nozzle, therefore different nozzle orifices were used for producing the ink patterns. The inverse value of the Ohnesorge number of the ink, an important parameter predicting its printability depending on the nozzle dimensions and the rheology of the ink, was verified to assess its printability in the different nozzles. When using piezo-electric ink-jet printing, it was possible to vary YBCO pattern dimensions from 40-200 µm in width and 200-250 nm in height on both buffered $SrTiO_3$ single crystals and buffered Ni-5at%W tape.

EXPERIMENTAL DETAILS

The aqueous precursor solution was prepared by dissolving $Y_2(CO_3)_3.1.9H_2O$ (99.9 %, Sigma Aldrich), $Ba(OH)_2.8H_2O$ (98 %, Janssen) and $Cu(NO_3)_2.2.5H_2O$ (98 %, Alfa Aesar) salts in water and nitrilo-triacetic acid (NTA, 99 %, Alfa Aesar). The addition of triethanolamine (99+ %, Acros Organics) increases the pH to 6-8 and the viscosity to 6.79 mPa s (22 °C, shear rate of 9.10^4 s^{-1}, Haake Technik rheometer) respectively. The total metal ion concentration of the precursor solution was 1.1 mol/L (0.185 mol/L YBCO), as verified by ICP-OES (Spectro, Genesis) [26].
The density of the aqueous solution was obtained using a 10 cm^3 glass pycnometer (Duran). The surface tension of the precursor solution and contact angles on different substrates were measured with a DSA30 instrument (KRÜSS, GmbH, Germany).
The as-received $SrTiO_3$ (STO, CrysTec) and CeO_2 - $La_2Zr_2O_7$ buffered Ni-5at%W (Deutsche Nanoschicht GmbH) substrates were cleaned in isopropanol prior to ink-jet printing in order to remove dust and organics, and dried in air.
The substrates were coated at room temperature using both a single and a multi-nozzle piezoelectric DOD ink-jet system. By applying pulses of a specific electrical waveform to the

piezoelectric actuators, the ink chamber is deformed resulting in a pressure wave, which draws ink into the region of the orifice and expels it, forming a drop in flight. A Dimatix materials printer (Fujifilm Dimatix Inc. DMP-2800), with cartridges providing orifice diameters of 9 and 23 µm (~ 1 and 10 picoliter droplets) respectively, was used as the multi-nozzle system; and for the single nozzle system, Microfab nozzles with a 30 and 60 µm orifice diameter (MicroFab Technologies, MJ-ABP-01-30) and an XY positioning system under computer control were selected. Drop formation and fluid behavior was also imaged in-situ during printing, using a camera (Allied Vision Technologies, Stingray F-125B) with a telecentric zoom lens (Moritex, MLZ07545) and strobed collimated LED illumination (bespoke, University of Cambridge). Custom-written software was used to control image acquisition and to quantitatively analyse the drop volume and velocity. The ink was filtered with a 0.2 µm pore size PET filter prior to printing. Printing was performed using a unidirectional raster pattern, with correct drop positioning achieved by computer-controlled synchronization of the movement of the printer nozzle and ink jetting. All samples were dried at 120 °C in air.

Subsequently, the samples on $SrTiO_3$ were heat treated at 20 °C/min from room temperature to 780 °C in a humid 100 ppm O_2/N_2 atmosphere, and a maximum temperature of 760 °C was selected for patterns deposited on buffered tape [26, 32]. After 90 min dwell time, the gas was switched to dry 100 ppm O_2/N_2 for 40 minutes. Afterwards, the temperature was decreased to 400 °C at 10 °C/min. During this cooling stage, a gas switch to pure O_2 took place at 520 °C. After annealing for 60 min, the samples were furnace cooled to room temperature.

The crystallinity of the processed films was verified using X-ray diffraction (Bragg-Brentano configuration, Siemens, D5000; Cu-Kα). The sample morphology was characterized using optical microscopy (Leitz, Laborlux 12 POL S) and SEM (FEI Nova 600 Nanolab Dual-Beam FIB). A cross section of the layers was made using the FIB module coupled with SEM to verify the thickness of the layers. The shape of the multi-filamentary patterns was visualized by using optical profilometry (Veeco, NT9080). The critical temperature of the superconducting patterns was measured by resistivity measurements using a custom-made four-point test device (Keithly).

DISCUSSION

In recent years, a lot of research has been dedicated to the development of low cost, fluorine-free, preferably aqueous precursor solutions for the chemical deposition of YBCO and buffer layers [33-36]. We have recently published that the use of chelating agents such as NTA and triethanolamine to increase the ion solubility can lead to excellent YBCO precursors [26, 37]. While initially the optimization of the ratio of the chelating agents versus metal ion concentration and the pH were mostly done by trial and error and extensive lab work, we have shown later that it is possible to obtain a better insight into the chemistry by using both theoretical speciation distributions and experimental data obtained by electron paramagnetic resonance (EPR) revealing the related coordination chemistry. In our case we found that a NTA : total metal concentration ratio of 0.45 and a pH range of 6 to 7 were the most suitable formulations leading to precursor solutions with a total metal concentration of 1.1 mol/L that are stable for several months.

In order to have a better insight into the ink printability, we need to ensure that the physical properties of the ink fulfill the criteria for ink-jet printing. The pressure wave inside the print head needs to overcome the viscous flow and the surface tension of the ink. If the viscosity is too high, the pressure wave is damped, inhibiting the jetting of an ink droplet. The generation of

droplets in a DOD printer is a complex process, and the precise physics and fluid mechanics of the process are the subject of much research. The behavior of inks in the printing system can be quantified by a number of dimensionless groupings of physical constants, i.e. the Reynolds (Re), Weber (We) and Ohnesorge (Oh) numbers:

$$\mathrm{Re} = \frac{vl\rho}{\eta}, We = \frac{v^2 l\rho}{\sigma}, Oh = \frac{\sqrt{We}}{\mathrm{Re}} = \frac{\eta}{\sqrt{\sigma\rho l}} \quad (1)$$

with σ, ρ, η and v the ink surface tension, density, viscosity and velocity respectively and l the diameter of the orifice of the nozzle. The Reynolds number is a ratio of internal and viscous forces and the Weber number represents the ratio between the internal and surface tension forces. The inverse value of the Ohnesorge number is a characteristic value which is independent of the droplet velocity. It has been observed that Oh^{-1} should be higher than 2 to ensure proper ink jetting, and more recently Reis and Derby proposed a range of $1 < Oh^{-1} < 10$ [29, 38]. The lower limit is a result of the viscous dissipation of the pressure wave and the upper limit indicates the region in which the formation of satellite drops dominates over a single droplet. This upper limit can be relaxed, as long as the satellites merge with the main droplet before impact on the substrate.

In Table I we show the fluid properties determined for the aqueous YBCO ink used in this work. Since different printing systems are used, the inverse Ohnesorge numbers for the different orifice diameters are presented in Table II.

Table I. Fluid properties of the YBCO ink.

Surface tension σ [J m^{-2}]	Density ρ [kg m^{-3}]	Viscosity η [Pa s]
6.79 x 10^{-2}	1233	6.8 x 10-3

Table II. Different printing systems used with the corresponding inverse Ohnesorge number for the YBCO ink.

Printing system	Nozzle diameter l (x 10^{-6} m)	Oh^{-1}
DMP2800	9	4.04
	23	6.31
Microfab	30	7.37
	60	10.42

In order to examine the droplet formation process, drop visualization was performed using the Microfab (30 and 60 μm) piezoelectric nozzles and in-house written software. An anti-symmetric bipolar waveform was applied to the piezoelectric element with a maximum voltage of 16 V and 22 V for the 30 μm and 60 μm orifices respectively. From figure 1a, one can see the different stages during ink-jet printing. In the first stage, a growing filament is visible, where after some time, the formation of a droplet starts due to the surface tension forces of the ink. The droplet remains attached to the nozzle by an elongated filament. The detachment of the filaments begins at the nozzle, creating a tail behind the ejected droplet. The relatively high surface tension of the

aqueous ink ensures the recombination of the tail with the main drop. Also visible in figure 1a are the secondary oscillations of the ink due to the propagation of the wave pulse in the ink chamber. With the software, both droplet velocity and total volume can be calculated as shown in figure 1b. One droplet contains 90 pL of ink.

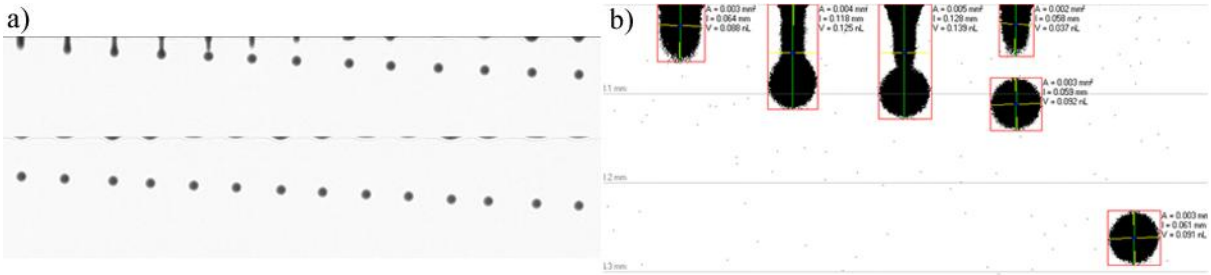

Figure 1. (a) Jetting analysis for the YBCO ink, using a 60 µm Microfab nozzle fired at 22 V with 5 µs time intervals with a final travelled distance of 340 µm and (b) highlighting the important phases during the jetting, images taken at delay times of 35, 65, 75, 85 and 205 µs.

Multi-nozzle printing was performed with the Dimatix materials Printer. This printer has a built-in camera for drop watching which can be used for calculating the trajectory velocity of the droplet as represented in figure 2. The standard waveform consists of a negative voltage peak to suck ink into the ink chamber, a maximum positive voltage to dispense the ink and a segment that allows the nozzle to recover to its original shape without sucking air in the chamber. We found that for the 1 pL and the 10 pL cartridges, the use of a maximum voltage of 8.2 V and 11 V at 33 °C resulted in satellite free droplet formation.

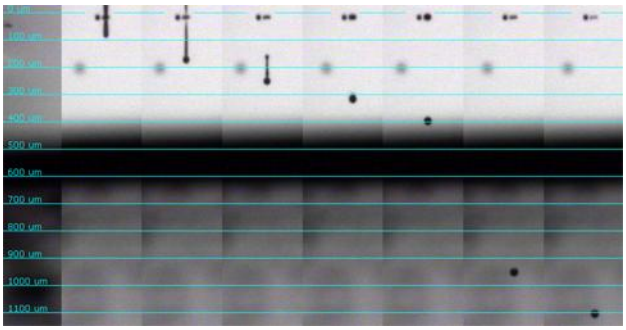

Figure 2. Jetting analysis for the YBCO ink at 11 V and 33 °C, using a 10 pL DMP cartridge.

After finding the best suited jetting parameters, i.e. no satellite formation and a well-defined vertical droplet trajectory, the wetting of the ink onto the different substrates needs to be characterized and optimized. As published before, this can be done by using the pendant drop method for optically determining the surface tension (σ) of the ink and also by measuring the different contact angles (θ_{eqm}) of the ink on the substrates [26]. The surface tension of the substrate was determined by measuring the contact angle for water and diiodomethane. Using these methods, the wetting behavior of the ink on both the single crystal $SrTiO_3$ (STO) and the buffered Ni-5at%W substrates could be quantified (Table III). The large uncertainty (from 5 – 10 °) in the contact angle values is due to local dewetting effects on the substrate and for further analysis, an upper bound contact angle of 10 ° was used, since the worse value will determine the maximum inter-droplet distance during printing.

Table III. Surface tension and wetting behavior of the YBCO ink and the substrates used.

Liquid / Solid	σ [mN/m]	σ_{polar} [mN/m]	$\sigma_{dispersive}$ [mN/m]	θ_{eqm} [degrees]
STO	77.9	34.6	43.3	5 – 10
Buffered tape [a]	77.8	33.5	45.3	10 – 15
YBCO solution	67.9	41.9	26	/
[a] Ni-5%W tape / LZO / LZO / CeO_2				

When combining the knowledge of the wetting behavior of the ink on the different substrates and the droplet dimensions, it now becomes possible to predict the pattern dimensions using equation 2 [29].

$$d_{con} = d_0 \left(\frac{8}{\tan\frac{\theta_{eqm}}{2}\left(3+\tan^2\frac{\theta_{eqm}}{2}\right)} \right)^{1/3} \quad (2)$$

Where d_{con}, d_0 and θ_{eqm} are the droplet diameter after contact onto the substrate, the droplet diameter in flight and the contact angle at equilibrium. Using this equation, the minimum width (equal to d_{con}) of a pattern can be predicted. In order to increase the thickness of the YBCO filament, several successive coatings were deposited, without an intermediate drying step. In Table 4, we summarized the data for the different nozzles used for printing the YBCO ink onto $SrTiO_3$ substrates. A large difference in the droplet speed in flight (υ) can be observed for Dimatix versus Microfab printing. This is probably due to the differently constructed nozzles and to variations in the wave-form. After calculating the droplet diameter in flight, the droplet diameter after contact was calculated using equation 2 and a contact angle of 10 °. This value was then used for predicting the inter-droplet distance (IDD) that should be used for printing. Although the inter-droplet distance was chosen to have a slightly lower value than d_{con}, the pattern width did not increase when using the 9 and the 22 µm nozzles orifices. For the others, a larger variation was observed in the line width. This can be due do the lower repeatability doing the multiple coatings and due to the local wetting differences. A 5 ° contact angle would result in a spreading of 220 µm starting from a d_0 = 61 µm.

Table IV. Summary of the data for printing YBCO ink onto $SrTiO_3$ substrates.

Φ orifice [µm]	volume [pL]	υ [m s^{-1}]	Re	We	d_0 [µm]	d_{con} [µm]	IDD [µm]	line width [µm]	# coatings
9	1	/	/	/	12.4	38	29	**40**	7
22	10	7.86	31.4	24.7	28	87	44	**90**	7
30	22	1.68	9.1	1.5	40	125	100	**160 ± 25**	4
60	90	1.24	13.5	1.7	61	190	140	**190 ± 30**	4

Even when depositing multiple coatings on top of each other, the line width after thermal processing is in good agreement with the predicted value.
Figure 3 shows the digital photographs and optical profilometry images for the different samples. Fine, straight and well-separated filaments exhibiting almost no coffee-ring effect can be observed. Local dewetting effects present sample b and c need to be prevented in the future in order to have a continuous pattern. Breaks in a few filaments would simply reduce the current-carrying cross-sectional area slightly in short samples, but this issue must be addressed for long-length production to be feasible. When taking a closer look at the pattern shape, nice straight edges and a homogeneous thickness distribution are found. The pattern width ranges from 40 to 190 µm as summarized in Table IV. The YBCO tracks have a thickness between 100 and 250 nm after full thermal processing. The distance between the different lines is between 150 and 200 µm. With these distances it becomes possible to divide the YBCO coating into 49, 32, 24 and 24 lines for a 10 x 10 mm single crystal substrate. This is important because it is reported in the literature that the hysteresis losses will be decreased by the inverse of the number of lines ($1/N_a$) in comparison with a completely covered substrate [15, 22]. The currently reported width for patterns is going from 30 µm up to one millimeter when using lithography or etching methods [7, 8, 12, 11, 16, 19, 21, 22, 24]. With our ink-jet printing technique we can obtain a similar lateral resolution in only one processing step. Since the reported YBCO thickness is around 1 µm, modifications to the ink, the deposition parameters and the thermal process will be necessary in order to exceed the 200 nm that we currently obtain.

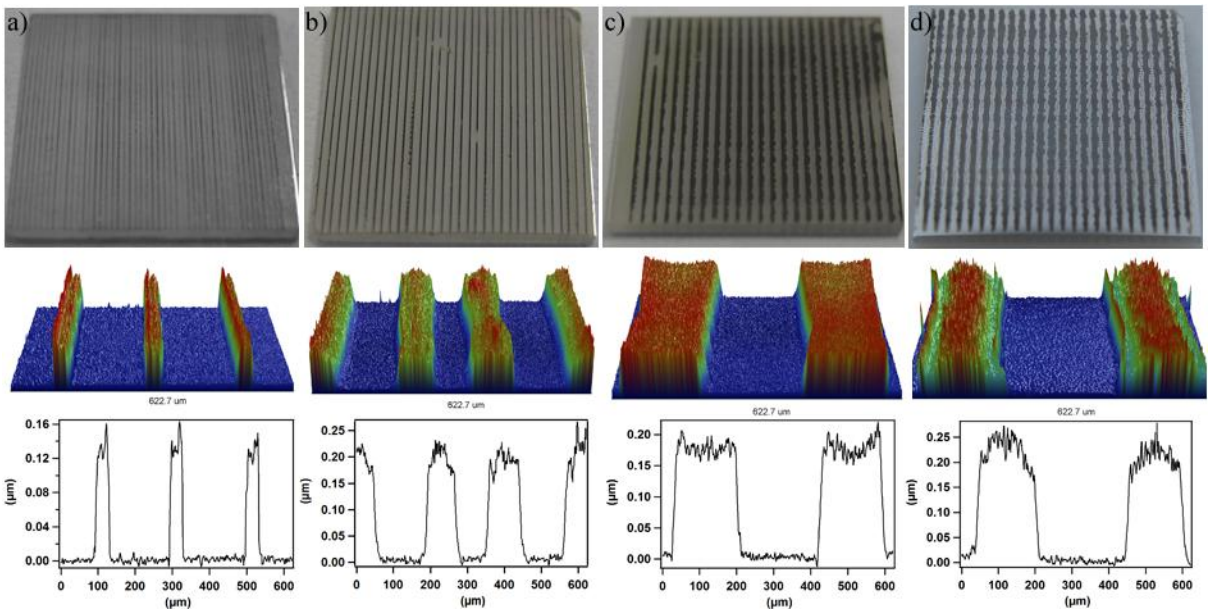

Figure 3. (Top) Optical images, (middle) 3D and (bottom) 2D line scans obtained through optical profilometry for YBCO printed on 10 x 10 mm $SrTiO_3$ substrates with nozzles with from (a) to (d), a 9, 22, 30 and 60 µm orifice diameter respectively.

The crystallinity of the YBCO patterns after thermal processing was verified using θ-2θ X-ray diffraction (figure 4a). It can be seen that the preferred (00l) reflections are dominant on the $SrTiO_3$ substrate, but also some reflections indicative of the presence of a $BaCuO_x$ phase (*). This phase is often observed on the surface of the YBCO films, deposited by a chemical solution deposition method [26]. The weak reflections appearing at 20.5°, 41.8° and 21.8°, 44.5° and

44.9° are satellites of the large STO substrate peaks due to W-$L_{\alpha 1}$ and Cu-K_{β} radiation respectively.
The resistivity measurement obtained for ink-jet printed YBCO patterns, using the 60 µm nozzle, on $SrTiO_3$, is shown in figure 4b. Three lines were connected using silver paste. The measurement was performed in liquid nitrogen and results in a superconducting transition with a $T_{c,onset}$ of 88.6 K and a ΔT_c of 1.4 K. The resistivity does not decrease completely to zero, which may be due to the presence of the $BaCuO_x$ phase.

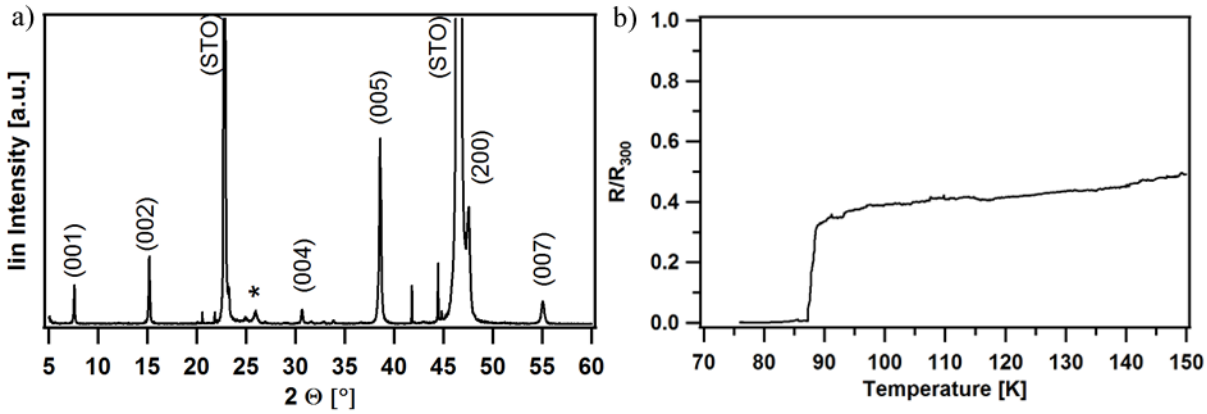

Figure 4. θ/2θ XRD spectrum (a) and resistivity measurements (b) of ink-jet printed YBCO patterns using the 60 µm Microfab nozzle on $SrTiO_3$ single crystal substrate after full thermal treatment.

Using the same 60 µm nozzle, the printing experiments were repeated on CeO_2-$La_2Zr_2O_7$-Ni-5at%W tape. Preliminary analysis has been performed on these samples. Optical profilometry revealed a line width of 170 ± 20 µm, and FIB-SEM cross-sectional analysis confirms the line thickness to vary between 220 to 250 nm, which is in good agreement with the predicted values using equation 2 and with the dimensions found for the same patterns printed on single crystal substrates.

CONCLUSIONS

Multi-filamentary YBCO patterns were successfully deposited on both $SrTiO_3$ and buffered Ni-5at%W tape using two set-ups of DOD piezo-electric ink-jet printers and a water-based YBCO ink. We are able to predict the pattern dimensions using knowledge of both the ink-jet printing parameters, jetting behavior, ink rheology and wettability on the selected substrates. The jettability of the ink was verified different nozzles by determining the inverse Ohnesorge number. After optimizing the inter-droplet distance and the number of successive coatings, tracks of 40 to 200 µm wide and 100 to 200 nm thick were obtained after full thermal processing. These tracks exhibit sharp edges and are very homogeneous in their overall profile, showing almost no coffee ring effect. After thermal processing, the patterns show strong c-axis oriented YBCO resulting in a $T_{c,onset}$ of 88.6 K and a ΔT_c of 1.4 K when performing resistivity measurements on the 200 µm wide sample. Further optimization of the printing process will be performed to further increase the pattern thickness while keeping the width constant and avoiding random YBCO formation.

REFERENCES

1. Zhang, W.; Rupich, M. W.; Schoop, U.; Verebelyi, D. T.; Thieme, C. L. H.; Li, X.; Kodenkandath, T.; Huang, Y.; Siegal, E.; Buczek, D.; Carter, W.; Nguyen, N.; Schreiber, J.; Prasova, M.; Lynch, J.; Tucker, D.; Fleshler, S., Physica C **2007,** *463–465*, 505-509.
2. Iijima, Y.; Kakimoto, K.; Sutoh, Y.; Ajimura, S.; Saitoh, T., Physica C **2004,** *412–414, Part 2*, 801-806.
3. Shiohara, Y.; Kitoh, Y.; Izumi, T., Physica C **2006,** *445–448*, 496-503.
4. Van Driessche, I.; Feys, J.; Hopkins, S. C.; Lommens, P.; Granados, X.; Glowacki, B. A.; Ricart, S.; Holzapfel, B.; Vilardell, M.; Kirchner, A.; Baecker, M., SUST **2012,** *25* (6), 065017 (12p).
5. Selvamanickam, V.; Chen, Y.; Xiong, X.; Xie, Y. Y.; Martchevski, M.; Rar, A.; Qiao, Y.; Schmidt, R. M.; Knoll, A.; Lenseth, K. P.; Weber, C. S., IEEE Trans. Appl. Supercond. **2009,** *19* (3), 3225-3230.
6. Iijima, Y.; Hosaka, M.; Sadakata, N.; Saitoh, T.; Kohno, O.; Takeda, K., Appl Phys Lett **1997,** *71* (18), 2695-2697.
7. Cobb, C. B.; Barnes, P. N.; Haugan, T. J.; Tolliver, J.; Lee, E.; Sumption, M.; Collings, E.; Oberly, C. E., Physica C **2002,** *382* (1), 52-56.
8. Majoros, M.; Glowacki, B. A.; Campbell, A. M.; Levin, G. A.; Barnes, P. N.; Polak, M., IEEE Trans. Appl. Supercond. **2005,** *15* (2), 2819-2822.
9. Sumption, M. D.; Coleman, E. L.; Cobb, C. B.; Barnes, P. N.; Haugan, T. J.; Tolliver, J.; Oberly, C. E.; Collings, E. W., IEEE Trans. Appl. Supercond. **2003,** *13* (2), 3553-3556.
10. Carr, W. J.; Oberly, C. E., IEEE Trans. Appl. Supercond. **1999,** *9* (2), 1475-1478.
11. Oberly, C. E.; Razidlo, B.; Rodriguez, F., IEEE Trans. Appl. Supercond. **2005,** *15* (2), 1643-1646.
12. Amemiya, N.; Kasai, S.; Yoda, K.; Jiang, Z. N.; Levin, G. A.; Barnes, P. N.; Oberly, C. E., SUST **2004,** *17* (12), 1464-1471.
13. Oberly, C. E.; Long, L.; Rhoads, G. L.; Carr, W. J., Cryogenics **2001,** *41* (2), 117-124.
14. Tsukamoto, O.; Sekine, N.; Ciszek, M.; Ogawa, J., IEEE Trans. Appl. Supercond. **2005,** *15* (2), 2823-2826.
15. Glowacki, B. A.; Majoros, M., SUST **2000,** *13* (7), 971-973.
16. Sumption, M. D.; Barnes, P. N.; Collings, E. W., IEEE Trans. Appl. Supercond. **2005,** *15* (2), 2815-2818.
17. Goldacker, W.; Frank, A.; Heller, R.; Schlachter, S. I.; Ringsdorf, B.; Weiss, K. P.; Schmidt, C.; Schuller, S., IEEE Trans. Appl. Supercond. **2007,** *17* (2), 3398-3401.
18. Badcock, R. A.; Long, N. J.; Mulholland, M.; Hellmann, S.; Wright, A.; Hamilton, K. A., IEEE Trans. Appl. Supercond. **2009,** *19* (3), 3244-3247.
19. Suzuki, K.; Yoshizumi, M.; Izumi, T.; Shiohara, Y.; Iwakuma, M.; Ibi, A.; Miyata, S.; Yamada, Y., Physica C **2008,** *468* (15-20), 1579-1582.
20. Sumption, M. D.; Collings, E. W.; Barnes, P. N., SUST **2005,** *18* (1), 122-134.
21. Abraimov, D.; Gurevich, A.; Polyanskii, A.; Cai, X. Y.; Xu, A.; Pamidi, S.; Larbalestier, D.; Thieme, C. L. H., SUST **2008,** *21* (8), 082004 (4 p).
22. Duckworth, R. C.; Paranthaman, M. P.; Bhuiyan, M. S.; List, F. A.; Gouge, M. J., IEEE Trans. Appl. Supercond. **2007,** *17* (2), 3159-3162.

23. Minsoo, K.; Freyhardt, H. C.; Lee, T. R.; Jacobson, A. J.; Galstyan, E.; Usoskin, A.; Rutt, A., IEEE Trans. Appl. Supercond. **2013,** *23* (3), 6601304 (4 p).
24. Kopera, L.; Smatko, V.; Prusseit, W.; Polak, M.; Semerad, R.; Strbik, V.; Souc, J., Physica C **2008,** *468* (24), 2351-2355.
25. Glowacki, B. A.; Mouganie, T., Inst. Phys. Conf. Ser. **2003,** *No. 181*, 1884.
26. Feys, J.; Vermeir, P.; Lommens, P.; Hopkins, S. C.; Granados, X.; Glowacki, B. A.; Baecker, M.; Reich, E.; Ricard, S.; Holzapfel, B.; Van Der Voort, P.; Van Driessche, I., J. Mater. Chem. **2012,** *22*, 3717–3726.
27. Tekin, E.; Smith, P. J.; Schubert, U. S., Soft Matter **2008,** *4* (4), 703-713.
28. Windle, J.; Derby, B., J Mater Sci Lett **1999,** *18* (2), 87-90.
29. Derby, B., In *Annual Review Of Materials Research*, Annual Reviews: Palo Alto, 2010; Vol. 40, pp 395-414.
30. Arin, M.; Lommens, P.; Hopkins, S. C.; Pollefeyt, G.; Van der Eycken, J.; Ricart, S.; Granados, X.; Glowacki, B. A.; Van Driessche, I., Nanotechnology **2012,** *23* (16), 165603 (10p).
31. Mouganie, T.; Glowacki, B. A., J Mater Sci **2006,** *41* (24), 8257-8264.
32. Vermeir, P.; Feys, J.; Schaubroeck, J.; Verbeken, K.; Baecker, M.; Van Driessche, I., Mater. Chem. Phys. **2012,** *133* (2-3), 998-1002.
33. Van Driessche, I.; Penneman, G.; De Meyer, C.; Stambolova, I.; Bruneel, E.; Hoste, S.; Ttp, In *Euro Ceramics Vii, Pt 1-3*, 2002; Vol. 206-2, pp 479-482.
34. Penneman, G.; Van Driessche, I.; Bruneel, E.; Hoste, S., In *Euro Ceramics Viii, Pts 1-3*, Mandal, H. O. L., Ed. 2004; Vol. 264-268, pp 501-504.
35. Cloet, V.; Cordero-Cabrera, M. C.; Mouganie, T.; Glowacki, B. A.; Falter, M.; Holzapfel, B.; Engell, J.; Backer, M.; Van Driessche, I., Science and Engineering of Novel Superconductors **2006**, 153-158.
36. Vermeir, P.; Deruyck, F.; Feys, J.; Lommens, P.; Schaubroeck, J.; Van Driessche, I., J. Sol-Gel Sci. Techn. **2012,** *62* (3), 378-388.
37. Lommens, P.; Feys, J.; Vrielinck, H.; De Buysser, K.; Herman, G.; Callens, F.; Van Driessche, I., Dalton Trans. **2012,** *41* (12), 3574-3582.
38. Fromm, J. E., IBM J Res Dev **1984,** *28* (3), 322-333.